

# The effect of mechanical activation on the carbothermic reduction kinetics of hematite-graphite mixture

F. Mohseni<sup>1\*</sup>, M. H. Abbasi<sup>2</sup> and M. Panjepour<sup>3</sup>

*Department of Materials Engineering, Isfahan University of Technology, Isfahan 8415683111, Iran.*

## Abstract

The effect of mechanical activation on structural changes and kinetics of carbothermic reduction of hematite with graphite was studied in this research. Hematite powder mixture with graphite (with stoichiometry ratio C/O=1) was milled for the time periods of zero to 50 hours, and the structural changes were studied using X ray diffraction (XRD). The effect of mechanical activation on the kinetics of hematite carbothermic reduction was studied by performing thermal analysis tests and by employing model-free and constant slope methods. The activation energy as well as the reaction mechanism was then determined. The results showed that by mechanical activation for a time period of 50 h, the activation energy is decreased from 387 kJ/mol<sup>-1</sup> to 186 kJ/mol<sup>-1</sup>, and the starting temperature of the reaction is decreased from 1125 to 620°C. The Boudouard chemical reaction was determined as the rate controlling step.

*Keywords:* Mechanical activation, Thermal analysis, Kinetic analysis, Activation energy, Hematite, Carbothermic reduction.

## 1. Introduction

Reduction of iron oxides by solid carbonaceous materials has attracted the attention of many investigators in recent years<sup>1-12</sup>. One of the reasons for the tendency toward solid fuels is economization in energy consumption and environmental issues through reduction of CO<sub>2</sub> emissions<sup>2,10-13</sup>. In order to increase the production rate and energy efficiency, and to design and optimize the use of equipment, the study of kinetics of carbothermic reduction of iron oxides is of special importance<sup>14,15</sup>. For this purpose, extensive studies have been carried out on the effect of different factors such as mixture ratio, pattern of reduction (isothermal or nonisothermal conditions); particle size of iron oxide and carbon; their crystalline structure; and reduction temperature, etc. on this process<sup>1,3,9-11,16</sup>. Researchers unanimously agree that reducing the particle size of iron oxide and carbonaceous materials results in an increase in reduction rate<sup>1,3,6,8,17</sup>. One of the factors affecting the kinetics of the process of carbothermic reduction is the mechanical activation of reactant materials which have significant effects on the kinetics of the reactions by affecting the size of the particles and their structure. This process results in an increase in the contact surface area of the particles in the mixture,

surface energy increase due to the formation of new surface areas, and an increase in energy in crystalline defects and disorder, and crystallite refinement<sup>1,3-4,6,8,9</sup>. Therefore, in recent years special attention has been paid to the process of mechanical activation of iron oxides and solid reducing materials, and their effects on reduction reaction rate increase. Grohn et al.<sup>18</sup> in 1966 studied mechanochemical reduction of hematite with carbon at ambient temperature for the first time. Vahdati Khaki et al.<sup>3</sup> in 2002 studied the effect of milling on the rate of hematite reduction with graphite under argon atmosphere through thermal analysis method (TG-DTA). The results of this research showed that milling has significant effects on increasing the reduction rate and lowering the temperature. In 2004 Kashiwaya<sup>9</sup> reported that the production of nanoreactor phenomenon along with the transformation taking place in the crystalline structure and also the formation of reduction products during milling were the causes of this phenomenon. Also, Vahdati Khaki et al.<sup>3</sup> observed that graphite activation is more effective than iron oxide and this finding is in conformity with that reported by other researchers who believe that gasification reaction of carbon is the rate controlling of carbothermic reduction process<sup>3,5,10,11,19-20</sup>. Therefore, any factor resulting in a decrease in the activation energy of Boudouard reaction can improve the general rate of the reaction and can result in a decrease in energy consumption. Although extensive research works have been performed on the carbothermic reduction of iron oxides, calculation of kinetic parameters and the effect of mechanical activation require more research work. The goal

\*Corresponding author:

Tel: +98-913-2073584

Fax: +98 (311)3912752

E-mail: fmohseni2006@gmail.com

Address: Department of Materials Engineering, Isfahan University of Technology, Isfahan 8415683111, Iran.

1. M.Sc.

2. Professor

3. Assistant Professor

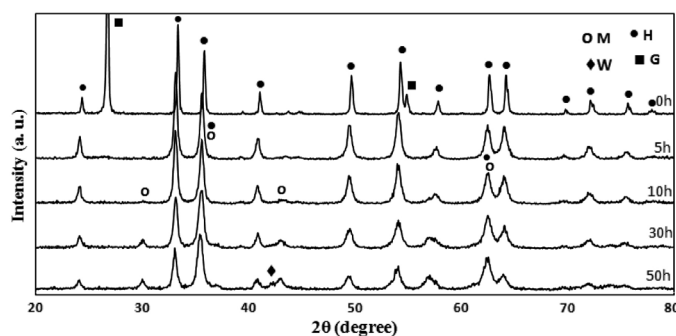


Fig. 1. XRD pattern of samples milled for different hours.

of this research is to study the effect of mechanical activation on kinetics of carbothermic reduction of hematite by using of several kinetic methods such as isoconversional methods and fitting method, the rate of changes, reaction temperature performance, activation energy, and reduction mechanism.

## 2. Materials and experimental methods

The raw materials included hematite powder with a purity of more than 99% manufactured by Merck Co.; and graphite powder with a purity of more than 99.9% with the average particle size of 10 $\mu$ m, manufactured by Fluca Co. To prepare the initial samples, cylindrical pellets with a diameter of about 2cm and height of about 0.5cm; under pressure of 14.7MPa for 0.5 h were prepared from hematite powder and were sintered at 1050 $^{\circ}$ C for 24 hours. The sintered pellets were then crushed into powder. The powder was then sieved and -53 $\mu$ m particles were used for subsequent mechanical milling. Powdery mixtures of hematite and graphite at stoichiometric ratio were milled in a planetary ball mill of Retch model PM100. (A steel vessel of 500cc volume, 12 steel balls with diameter of 20mm, ball to powder ratio 15:1, argon atm. and 250rpm).

XRD examination for phase analysis of milled and unmilled samples were performed using a Philips XPert X-ray diffraction with PW 3050 tube equipped with a Germanium monochromator in the diffracted beam arm and using Cu  $k\alpha$  radiation. The XRD pattern of samples was recorded in the range of  $2\theta = 20-80^{\circ}$  using a step size of  $0.05^{\circ}$  and a counting time of 1 s per step. The reduction process was studied by TG-DTA method in BAHF device with a resolution of 1 $\mu$ g. The approximate weight of the samples tested was about 30mg and the samples were heated at the heating rates of 10, 15, 20 $^{\circ}$ Cmin $^{-1}$  from room temperature to 1200 $^{\circ}$ C in crucibles made of alumina.

## 3. Results and discussion

### 3.1. Phase analysis

The XRD patterns of samples after different milling time periods are depicted in Fig. 1. It is observed that with an increase in milling time, the intensity of the peaks is decreased and their width is increased. Also, after 5h, the peak corresponding to graphite is

completely eliminated. The elimination of this peak is due to fast amorphization of graphite structure, which is a soft and laminated structure. The bond among the layers is weak and of Van der Waals type which is quickly broken due to impacts resulting from the balls transforming the main structure of graphite. Other researchers have also referred to such a case<sup>3,12,21</sup>.

Fig. 1 clearly depicts that with an increase in milling time period, the peak corresponding to magnetite appears and its intensity is increased. Also, at the time period of 50h. the peak corresponding to wustite appears (H, M, W and G refer to hematite, magnetite, wustite and graphite, respectively). So, it can be concluded that by milling, hematite particles are reduced to some extent, and magnetite and wustite phases are produced in the presence of carbon. Such phenomenon results from the presence of free and excited surfaces and high-energy transfer to the particles, causing mechanochemical transformations of hematite to lower iron oxides<sup>4,21-23</sup>.

Several methods are applicable for the determination of grain size and structural strain. Cauchy-Cauchy (Williamson-Hall), Cauchy-Gaussian and Gaussian-Gaussian are examples with the following equations, (Eq. 1-3)<sup>24-25</sup>.

$$\beta \cos \theta_0 = \frac{k\lambda}{d} + 2\varepsilon \sin \theta_0 \quad (1)$$

$$\frac{\beta^2}{\tan^2 \theta_0} = \frac{k\lambda}{d} \left( \frac{\beta}{\tan \theta_0 \sin \theta_0} \right) + 16\varepsilon^2 \quad (2)$$

$$\beta^2 \cos^2 \theta_0 = \left( \frac{k\lambda}{d} \right)^2 + 4\varepsilon^2 \sin^2 \theta_0 \quad (3)$$

Where  $\beta$  indicates the width of the peak at half maximum height,  $k$  is a constant ( $\sim 0.9$ ),  $\theta_0$  is the Bragg angle,  $d$  and  $\varepsilon$  refer to crystallite size and microstrain, respectively.

In this study by using Williamson-Hall equation and plotting  $\beta \cos \theta$  against  $\sin \theta$  for different peaks at different angles, a straight line was obtained and the grain size was calculated by the slope of the line and strain from its intercept. Fig. 2 shows the effect of milling time on hematite crystallite size and structural strain.

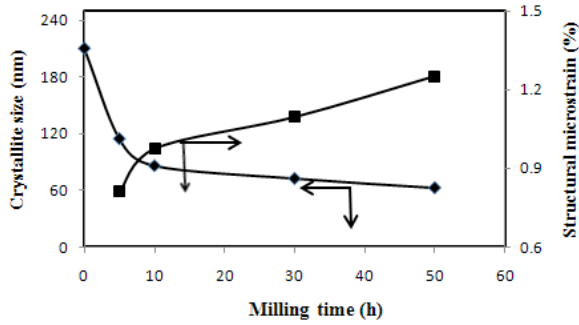


Fig. 2. The effect of milling time on hematite crystallite size and structural microstrain.

Fig. 2 clearly indicates that by increasing the milling time, the size of crystallites in hematite particles is reduced and structural strain is increased. Fig. 2 shows that by increasing the milling time up to 10h, the grain size is reduced to 85nm and to about 60nm in the 50h milled sample. Further milling has no significant effect. Fig. 2 shows that with an increase in milling time, the internal strain of hematite particles is increased up to 1.25% in the 50h milled sample. Fig. 3 depicts the SEM images of initial sample and Figs.4 and 5 show SEM images of the activated sample for time durations of 10 and 30h at two magnifications.

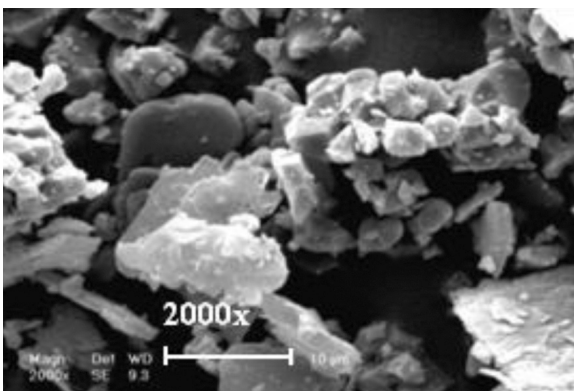
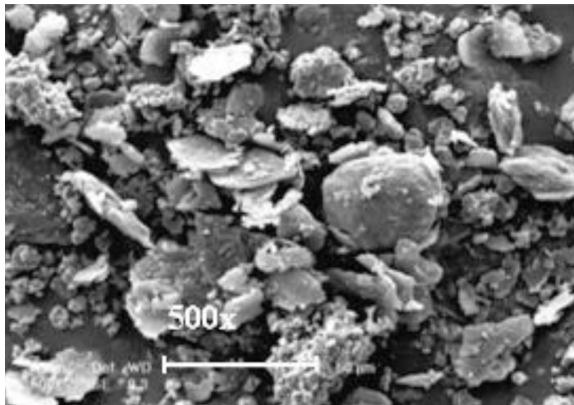


Fig. 3. SEM micrographs of hematite-graphite mixture before milling at two magnifications.

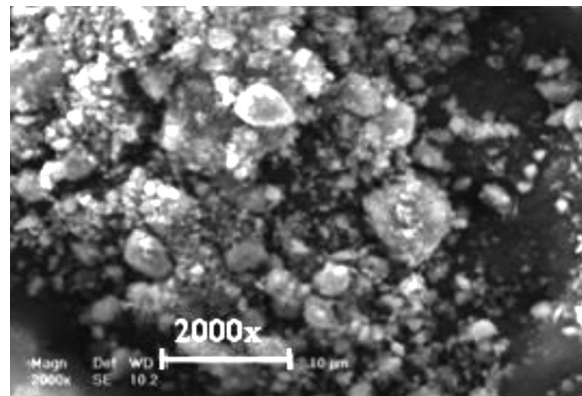
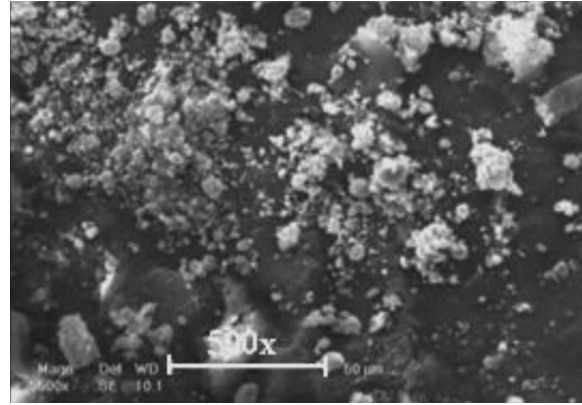


Fig. 4. SEM micrographs of hematite-graphite mixture milled for 10 hr at two magnifications.

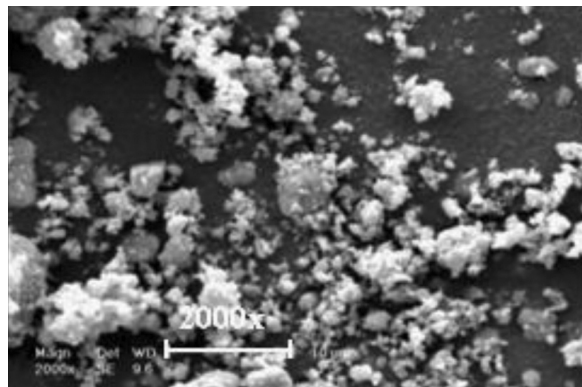
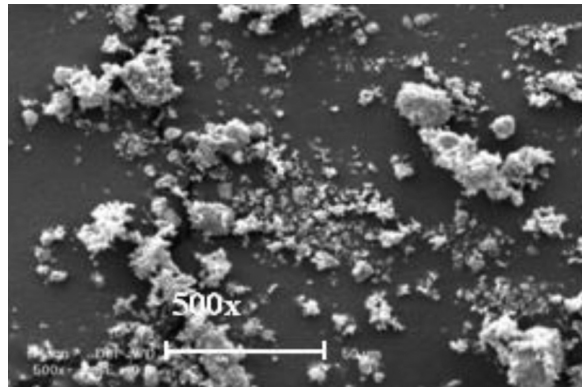


Fig.5. SEM micrographs of hematite-graphite mixture milled for 30 hr at two magnifications.

By comparing Figs 4 and 5, it is observed that by milling, the size of the particles is greatly reduced and the presence of agglomerates is increased. Fig. 5 clearly shows that during long periods of milling, close-packed agglomerate particles are formed which are impossible to be detected. The formation of compound structures taking place during long periods of milling corresponds to energy gathering phenomenon. In this state, the initial specifications of the powder mixture disappear, and due to structurally great compactness, the hard particles of hematite and magnetite are imprisoned in the soft particles of graphite<sup>6,9,21</sup>.

### 3.2. The concept of ( $\epsilon/d$ ) parameter

As referred to in section 3.1, the values of  $\epsilon$  and  $d$  of hematite particles in different samples changed depending on the time of milling which is due to the transfer of energy to the powder mixture. The transferred energy results in grain refinement and increase in internal strain. During mechanical milling  $d$  decreases while  $\epsilon$  increases. Therefore,  $\epsilon/d$  increases and could be considered as a criterion for mechanical activation<sup>21</sup>. The increase in  $\epsilon/d$  leads to reactivity improvement of the powder mixture while it positively affects the kinetics. Fig. 6 shows the variation of  $\epsilon/d$  values for hematite particles as a function of milling time.

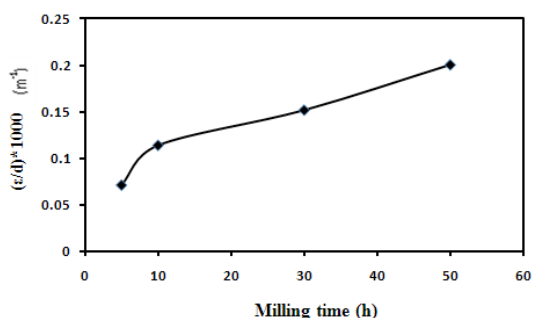


Fig. 6. The effect of milling time on the activation parameter ( $\epsilon/d$ ) for hematite particles.

### 3.3. Thermal characterization

The results obtained from TG-DTA tests are shown in Figs. 7-9. TG and RTG results are shown in Fig. 7 for the 50h milled sample with the heating rate of  $10^{\circ}Cmin^{-1}$ . Fig. 8 shows TG diagrams for the samples milled for different periods of time and constant heating rate of  $10^{\circ}min^{-1}$  and Fig. 9a and 9b show TG diagrams for 50h milled and unmilled samples at the rates of 10, 15 and  $20^{\circ}min^{-1}$ . The start and finish temperatures as well as maximum reaction rate of different samples are presented in Table 1. It is observed that with an increase in milling time, the start and finish reaction temperatures are reduced. This trend is more observable during shorter milling time periods. In other words, more increase in milling

time has no significant effect on lowering the reaction temperature.

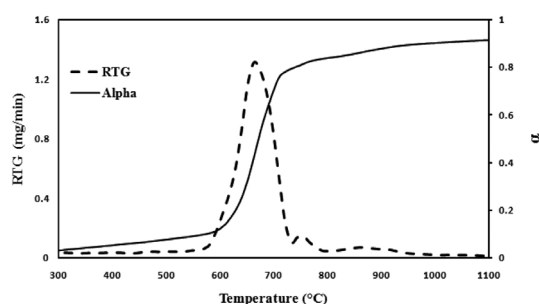


Fig. 7. The TG-RTG diagrams for 50 hr. milled sample.

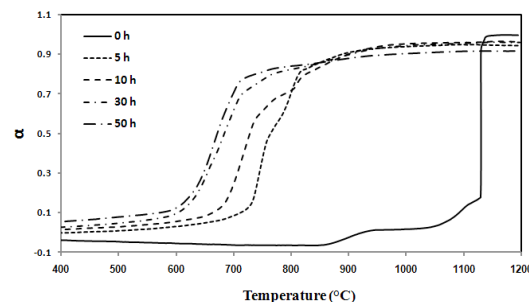


Fig. 8. The TG diagrams for the samples milled for different times.

Table 1. The start and finish temperatures and maximum rate of reduction as a function of milling time.

|       | $T_s$ (°C) | $T_f$ (°C) | $\Delta T$ (°C) | $R_{max}$ (mg/min) |
|-------|------------|------------|-----------------|--------------------|
| 0hr.  | 1125       | 1130       | -               | 4.38               |
| 10hr. | 680        | 766        | 86              | 1.309              |
| 30hr. | 625        | 725        | 100             | 0.999              |
| 50hr. | 620        | 709        | 89              | 1.316              |

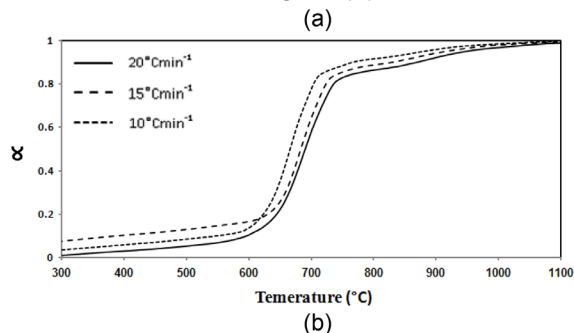
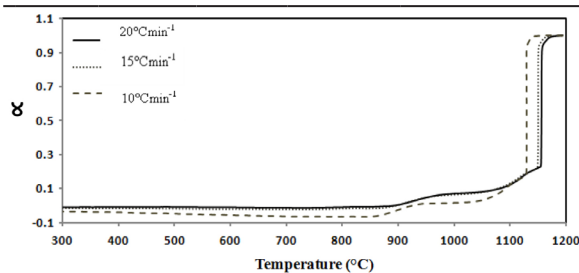


Fig. 9. TG diagrams of (a) unmilled and (b) milled for 50 hr samples.

That is because during long time periods of activation, the recovery phenomenon is also activated and the amount of the energy transferred to the powdery mixture is consumed by this phenomenon<sup>21)</sup>. By comparing TG diagrams corresponding to the activated samples by TG diagram of inactive sample, it is observed that the peaks related to reduction stages of hematite to magnetite and magnetite to wustite are eliminated, and the reduction process is done in one stage. With regard to the points discussed in sections 3.1, 3.2 and 3.3, it can be added that the cause of this phenomenon is the increase in the surface energy of the samples during activation; the presence of structural strain; the creation of structural defects such as dislocations; and in general an increase of internal energy level of the powdery mixture resulting in the overlap of reduction stages and elimination of middle ones.

### 3.4. Reduction kinetics

Many methods have been developed for the kinetic study of solid state reactions and determination of kinetic parameters using the data obtained from thermal analysis (TG-DTA). Although these methods are all valid from mathematical point of view, they are based on approximations which limit the use of these methods in certain conditions. Model-free or isoconversional methods are the most reliable methods for determination of activation energy. These methods are based on the fact that in thermal analysis (TG-DTA), the peaks corresponding to reaction performance are displaced by a change in heating rate of the samples, but the mechanism does not change. In other words, the reaction mechanism is not a function of the heating rate of the samples. Taking this assumption into account, the reaction rate at a specific conversion degree of the reaction is only a function of temperature<sup>26-28)</sup>. For a solid state reaction, the reaction rate can be expressed by Eq. 4.

$$\frac{d\alpha}{dt} \cong \beta \frac{d\alpha}{dT} = A \exp\left(-\frac{E}{RT}\right) \cdot f(\alpha) \quad (4)$$

Where  $\alpha$  is the conversion degree,  $\beta$  the heating rate ( $^{\circ}\text{Cmin}^{-1}$ ),  $T$  the absolute temperature (K),  $R$  the universal gas constant ( $\text{Jmol}^{-1}\text{K}^{-1}$ ),  $t$  the time (min),  $E$  the activation energy ( $\text{kJmol}^{-1}$ ),  $A$  is the pre-exponential factor and  $f(\alpha)$  is a function related to the reaction mechanism. It is proposed that the mechanism complexity be studied by determining  $E$  dependency on  $\alpha$  before the performance of any kinetic analysis<sup>14-15)</sup>. In general, the dependency of  $E$  on  $\alpha$  is recognized as an acceptable criterion for reaction mechanism complexity and isoconversional methods are the most successful for calculating  $E$ . If  $E$  is not dependent on  $\alpha$ , it can be concluded that the mechanism is a single-stage one; otherwise, the mechanism consists of stages<sup>14-15,27-28)</sup>.

### 3.4.1. Determination of activation energy by using model-free methods

To determine the activation energy for reduction process, two inactivated and 50h. activated samples were tested by TG-DTA analysis at three rates of heating ( $10, 15, 20^{\circ}\text{Cmin}^{-1}$ ). Kissinger-Akahira-Sunose (KAS) and Flynn-Wall-Ozawa (FWO) methods were employed to determine the activation energy<sup>29-30)</sup>.

FWO method is a linear integral method based on Eq. 5:

$$\log\beta = \log \frac{AE_{iso}}{Rg(\alpha)} - 2.315 - 0.4567 \frac{AE_{iso}}{RT} \quad (5)$$

Where KAS method is based on Eq. 6:

$$\ln \frac{\beta}{T^2} = \ln \frac{AR}{Eg(\alpha)} - \frac{E_{iso}}{RT} \quad (6)$$

By plotting diagrams  $\log\beta$  and  $\ln\beta/T^2$  against  $1/T$  for a fixed value of  $\alpha$  at different thermal rates, the values of  $E_{iso}$  are calculated from the slope of the lines. Figs. 10 and 11 show the results obtained. Also, activation energies obtained from KAS and FWO methods are summarized in Table 2.

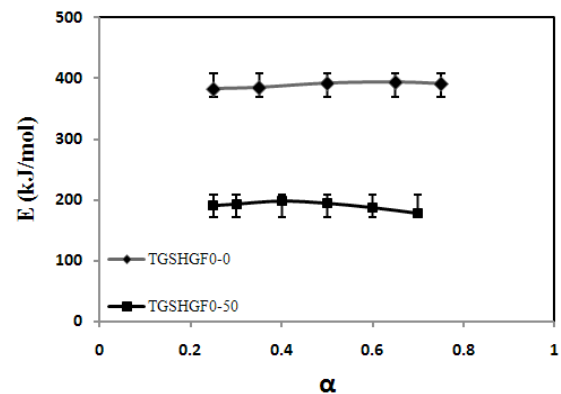


Fig. 10. Isoconversional activation energies for unmilled and milled for 50 hr samples by FWO method.

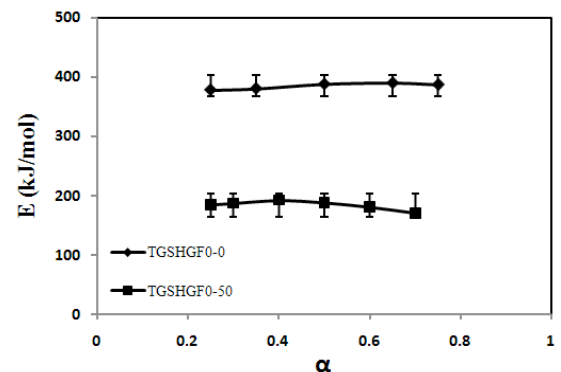


Fig. 11. Isoconversional activation energies for unmilled and milled for 50 hr samples by KAS method.

Table 2. The average values of  $E$  obtained by isoconversional methods of FWO and KAS.

|             | FWO<br>E(kJ/mol) | KAS<br>E(kJ/mol) |
|-------------|------------------|------------------|
| 50hr.milled | 189±7.37         | 183±7.88         |
| unmilled    | 387±4.79         | 384±5.03         |

### 3.4.2. Determination of activation energy by using constant slope method

This method is based on the assumption that diagram of  $\alpha$ -T can be divided into several regions with constant slopes<sup>31</sup>. The slope of each region shows the average rate of reaction and, being constant shows that the reaction controlling mechanism is fixed within this region. Thus,  $d\alpha/dT$  is constant in each region. By inserting this fixed value in Eq. 4, it can be rewritten as Eq. 8. By taking logarithm from the two sides, Eq. 9 is obtained in which  $f(\alpha)$  represents the reaction mechanism.

$$\frac{d\alpha}{dT} = C \quad (7)$$

$$\frac{C\beta}{A} = \exp\left(-\frac{E}{RT}\right) \cdot f(\alpha) \quad (8)$$

$$\ln(f(\alpha)) = \frac{E}{RT} + \ln\left(\frac{C\beta}{A}\right) \quad (9)$$

By plotting  $\ln f(\alpha)$  versus  $1/T$ , for different assumed reaction models, the best straight line represents the possible reaction mechanism. The value of the activation energy is then calculated from the slope of this line. The most common functions expressing the reaction mechanism are shown in table 3.

There is a possibility of linearization of several  $f(\alpha)$

functions. So, for decisive acceptance of the proposed model, the activation energy value obtained through the constant slope method is compared with the activation energy values obtained by model-free methods and a mechanism with the least difference in activation energy value is selected as the reaction mechanism. Shu et al. and Bonchon et al. [33-34] have employed a similar method to determine the kinetic parameters by the using Coats-Redfern (CR) method. Table 4 shows the kinetic parameters obtained from constant slope method using different models at heating rates of 10,15,20 °Cmin<sup>-1</sup>.

Table 4. kinetic parameters obtained by constant slope method.

| Mechanism              | E(kJmol <sup>-1</sup> ) | A(s <sup>-1</sup> )        |
|------------------------|-------------------------|----------------------------|
| F <sub>1</sub>         | 120                     | 8.8*10 <sup>5</sup>        |
| <b>F<sub>3/2</sub></b> | <b>180</b>              | <b>2.74*10<sup>9</sup></b> |
| F <sub>2</sub>         | 241                     | 8.81*10 <sup>12</sup>      |
| F <sub>3</sub>         | 361                     | 9.62*10 <sup>19</sup>      |
| D <sub>1</sub>         | 124                     | 1.62*10 <sup>6</sup>       |
| D <sub>2</sub>         | 176                     | 9.79*10 <sup>8</sup>       |
| D <sub>3</sub>         | 237                     | 7.94*10 <sup>11</sup>      |
| D <sub>4</sub>         | 197                     | 3.6*10 <sup>9</sup>        |

By comparing the data in Tables 3 and 4, it is observed that the activation energy obtained from chemical control model and the two-dimensional diffusion controlled model are in relatively good harmony with the activation energy obtained from model-free methods. Therefore, one of these two mechanisms should be considered as the mechanism for the performance of reduction reaction.

Table 3. Algebraic expressions of  $f(\alpha)$  and  $g(\alpha)$  for the reaction models<sup>32</sup>.

| No. | Symbol | Reaction model  | $f(\alpha)$                                | $g(\alpha)$                      |
|-----|--------|---|--|----------------------------------|
| 1   | P1     | Power law   | $4\alpha^{3/4}$                            | $\alpha^{1/4}$                   |
| 2   | P2     | Power law   | $3\alpha^{2/3}$                            | $\alpha^{1/3}$                   |
| 3   | P3     | Power law   | $2\alpha^{1/2}$                            | $\alpha^{1/2}$                   |
| 4   | P4     | Power law   | $2/3\alpha^{-1/2}$                         | $\alpha^{3/2}$                   |
| 5   | R1     | Zero-order (Polanyi-Winger equation)  | 1  | $\alpha$                         |
| 6   | R2     | Phase-boundary controlled reaction (contracting area, i.e., bidimensional shape)    | $2(1-\alpha)^{1/2}$                        | $[1-(1-\alpha)^{1/2}]$           |
| 7   | R3     | Phase-boundary controlled reaction (contracting volume, i.e., tridimensional shape) | $3(1-\alpha)^{2/3}$                        | $[1-(1-\alpha)^{1/3}]$           |
| 8   | F1     | First-order (Mampel)  | $(1-\alpha)$                               | $-\ln(1-\alpha)$                 |
| 9   | F3/2   | Three-halves order  | $(1-\alpha)^{3/2}$                         | $2[(1-\alpha)^{-1/2}-1]$         |
| 10  | F2     | Second-order  | $(1-\alpha)^2$                             | $(1-\alpha)^{-1}-1$              |
| 11  | F3     | Third-order   | $(1-\alpha)^3$                             | $(1/2)[(1-\alpha)^{-2}-1]$       |
| 12  | A3/2   | Avrami-Eroféev ( $n=1.5$ )  | $(3/2)(1-\alpha)[-\ln(1-\alpha)]^{1/3}$    | $[-\ln(1-\alpha)]^{2/3}$         |
| 13  | A2     | Avrami-Eroféev ( $n=2$ )  | $2(1-\alpha)[-\ln(1-\alpha)]^{1/2}$        | $[-\ln(1-\alpha)]^{1/2}$         |
| 14  | A3     | Avrami-Eroféev ( $n=3$ )  | $3(1-\alpha)[-\ln(1-\alpha)]^{2/3}$        | $[-\ln(1-\alpha)]^{1/3}$         |
| 15  | A4     | Avrami-Eroféev ( $n=4$ )  | $4(1-\alpha)[-\ln(1-\alpha)]^{3/4}$        | $[-\ln(1-\alpha)]^{1/4}$         |
| 16  | D1     | One-dimensional diffusion   | $1/2\alpha$                                | $\alpha^2$                       |
| 17  | D2     | Two-dimensional diffusion (bidimensional particle shape)<br>Valensi equation        | $1/[-\ln(1-\alpha)]$                       | $(1-\alpha)\ln(1-\alpha)+\alpha$ |
| 18  | D3     | Three-dimensional diffusion (tridimensional particle shape)<br>Jander equation      | $3(1-\alpha)^{1/3}/2[(1-\alpha)^{-1/3}-1]$ | $[1-(1-\alpha)^{1/3}]^2$         |
| 19  | D4     | Three-dimensional diffusion (tridimensional particle shape)<br>Ginstling-Bronstein  | $3/2[(1-\alpha)^{-1/3}-1]$                 | $(1-2\alpha/3)-(1-\alpha)^{2/3}$ |

### 3.5. Reduction mechanism

As it was pointed out in section 1, in many research works the rate controlling step has been considered as carbon gasification, i.e. chemical reaction. Also, the data in Table 2 show that the activation energy for the inactivated sample is close to the activation energy of Boudouard reaction<sup>35</sup>. It can therefore be predicted that the mechanism governing reduction process is a chemical reaction. Table 2 also shows that 50-hour mechanical activation lowers the activation energy from 387 to 186kJmol<sup>-1</sup> which is a significant reduction. Kashiwaya et al.<sup>9</sup> have pointed out that during long time milling of hematite and graphite, the graphite particles act as a soft bulk and the hematite particles are placed within the graphite bulk leading to a nano-reactor phenomenon which causes a decrease in the reduction temperature and activation energy. Researchers have pointed out that graphite activation, compared to hematite, is more effective on reduction kinetics<sup>3,8</sup>. They have also pointed out that the iron produced during direct reduction process is spongy and acts as a catalyst. The above-mentioned points all confirm that Boudouard chemical reaction is controlling the direct reduction reaction rate. Therefore, every factor affecting the improvement of Boudouard reaction rate and lowering the activation energy of this reaction can have positive effects on the reduction kinetics.

### 4. Conclusion

The kinetics of carbothermic reduction of milled and unmilled samples of hematite-graphite mixture was studied and compared using model-free (KAS and FWO) and constant slope methods. The following conclusions can be drawn from this work:

- With an increase in milling time up to 50 hours, the grain size of hematite was reduced to 62nm, but the structural strain increased 1.25%.
- By increasing the milling time to 10 hours, the magnetite peaks appeared in XRD patterns and with a further increase in the milling time, its intensity was increased. 50 hours of milling led to the formation of wustite.
- The activation energy for the inactivated sample was calculated to be about 385kJmol<sup>-1</sup> which is in conformity with the Boudouard reaction activation energy.
- Mechanical activation for 50 hours decreases the starting temperature of reduction from 1125 to 620°C and lowers the activation energy from about 385 to about 186kJmol<sup>-1</sup>.

- Calculation of activation energy of the activated and inactivated samples by model-free and constant slope methods and their comparison showed that the reaction was of chemical control type and the carbon gasification reaction was determined as the controlling step for the carbothermic reduction of hematite with graphite.

### References

- [1] Y. Kashiwaya and K. Ishii: ISIJ Int., 44 (2004), 1981.
- [2] Y. Kashiwaya, M. Kanabe and K. Ishii: ISIJ int., 46 (2006), 1610.
- [3] J. V. khaki, K. Ishii and H. Suzuki: ISIJ int., 42 (2002), 13.
- [4] Y. Kashiwaya, , H. Suzuki and K. Ishii: ISIJ int., 44 (2004), 1970.
- [5] J. Yang, T. Mori and M. Kuwabara: ISIJ int., 47 (2007), 1394.
- [6] J. V. Khaki, M.R. Aboutalebi and S. Raygan: Mineral Proc. Extract. Metall., 25 (2004), 29.
- [7] Y. Iguchi and Y. Takada: ISIJ Int., 44 (2004), 673.
- [8] I. Seki and K. Nagata: ISIJ Int., 46 (2006), 1.
- [9] Y. Kashiwaya, H. Susuki and K. Ishii: ISIJ Int., 44 (2004), 1975.
- [10] Y. Kashiwaya, Y. Yamaguschi, H. Kinoshita and K. Ishii, ISIJ int., 47 (2007), 226.
- [11] S. K. Dey, B. Jana and A. Basumallick: ISIJ int., 33 (1993), 735.
- [12] S. Raygan, J. V. Khaki and M.R. Aboutalebi: Mater. Synth. Proc., 10 (2002), 113.
- [13] G.M. Chowhhury and G.G. Roy: Comp. Mater. Sci., 45(2009), 176.
- [14] S.D. Genieva, L.T. Vlaev and A.N. Atanassov: J. Therm. Anal. Calorim., 99 (2010), 551.
- [15] N.S. Varandecic, M. Erceg, M. Jakic and I. Klaric: Thermochim. Acta., 498 (2010), 71.
- [16] J. V. Khaki, M. Panjepour, Y. Kashiwaya, K. Ishii and M. S. Bafghi: Steel Res. int., 75 (2004), 169.
- [17] P. Pourghahramani and E. Forssberg: Int. J. Miner. Process., 82 (2007), 96.
- [18] V.H. Grohn, R. Paudert and H. Friedrch: Zeitschrift fur anorganische und allgemeine Chemie Band, 384 (1966), 21.
- [19] S. Nath: Metall. Matr. Eng., (2009).
- [20] S. Ueda, K. Yanagiya, K. Watanabe, T. Murakami, R. Inoue and T. Ariyama: ISIJ int., 49 (2009), 827.
- [21] R. Tahmasbi, M. Shamanian, M. H. Abbasi and M. Panjepour: J. Alloys Compd., 472 (2009), 334.
- [22] M. Zdujic, C. Jovalekic, Lj. Karanovic and M. Mitric: Mater. Sci. Eng. A, 262 (1999), 204.
- [23] M. Zdujic, C. Jovalekic, Lj. Karanovic, M. Mitric, D. Poleti and D. Skala: Mater. Sci. Eng. A, 245 (1998), 109.

- [24] S.C. Tjong and H. Chen: *Mater. Sci. Eng. R*, 45 (2004), 1.
- [25] D. Oleszak, A. Olszjan: *Proc. of the XVIII Applied Crystallography Conference, Wisla, Poland*, (2000), 39.
- [26] M. Erceg, T. Kovacic and S. Perinovic: *Thermochim. Acta*, 476 (2008), 44.
- [27] S. Vyazovkin and C.A. Wight: *Thermochim. Acta*, 340-341 (1999), 53.
- [28] P. Pourghahramani and E. Forsberg: *Thermochim. Acta*, 454 (2007), 69.
- [29] T. Ozawa: *A New Method Of Analyzing Thermogravimetric Data*, 11 (1965), 1881.
- [30] H. Kissinger: *Analytical Chemistry National Bureau of Standards, Washington, D. C.* 29 (1957), 1072.
- [31] A. Maleki, M. Panjepour, B. Niroumand and M. Meratian, *J. Mater. Sci.*, (2010).
- [32] B. Jankovic, B. Adnadevic and J. Jovanovic: *Thermochim. Acta*, 452 (2007), 106.
- [33] B. Boonchom and S. Puttawong: *Physica B.*, 405 (2010), 2350.
- [34] Q. Shu, J. Liu, J. Zhang and M. Zhang: *Metal.*, 13 (2006), 1.
- [35] R. Padilla, M.C. Ruzi and H.Y. Sohn: *Metall. Mater. Trans. B*, 28 (1997), 265.